Experimental Observation of the Ground-State Geometric Phase of Three-Spin *XY* Model

2016 Chinese Phys. Lett. 33 060301

(http://iopscience.iop.org/0256-307X/33/6/060301)

Experimental Observation of the Ground-State Geometric Phase of Three-Spin XY Model *

Hui Zhou(周辉)[1], Zhao-Kai Li(李兆凯)[1,2**], Heng-Yan Wang(王恒岩)[1], Hong-Wei Chen(陈宏伟)[3], Xin-Hua Peng(彭新华)[1,2**], Jiang-Feng Du(杜江峰)[1]

[1]*Hefei National Laboratory for Physical Sciences at the Microscale and Department of Modern Physics, University of Science and Technology of China, Hefei 230026*

[2]*Synergetic Innovation Center of Quantum Information and Quantum Physics, University of Science and Technology of China, Hefei 230026*

[3]*High Magnetic Field Laboratory, Hefei Institutes of Physical Science, Chinese Academy of Sciences, Hefei 230031*

(Received 14 March 2016)

The geometric phase has become a fundamental concept in many fields of physics since it was revealed. Recently, the study of the geometric phase has attracted considerable attention in the context of quantum phase transition, where the ground state properties of the system experience a dramatic change induced by a variation of an external parameter. In this work, we experimentally measure the ground-state geometric phase of the three-spin XY model by utilizing the nuclear magnetic resonance technique. The experimental results indicate that the geometric phase could be used as a fingerprint of the ground-state quantum phase transition of many-body systems.

PACS: 03.65.Vf, 05.30.Rt, 76.60.−k, 64.70.−p DOI: 10.1088/0256-307X/33/6/060301

Discovered by Berry in 1984,[1] the wave function of a quantum system will acquire an extra phase (namely Berry's phase) in addition to the usual dynamical phase under the condition that the Hamiltonian is cyclic and adiabatic. This phase is also known as the geometric phase since the phase factor depends only on the geometry of the evolutionary path in parameter space. Further study indicates that this phenomenon also exists in the noncyclic,[2] nonadiabatic evolution,[3] and the case of mixed states.[4,5] The geometric phase has been experimentally observed in many systems, e.g., photons,[6] spin-polarized neutrons,[7] nuclear magnetic resonance[8] and superconducting systems.[9] Now the applications of the geometric phase can be found in various fields.[10−12] Recently, the relationship between the geometric phase and quantum phase transition (QPT) has been revealed gradually and increasing interest has been drawn to the role of the geometric phase in characterizing QPT of many-body systems.[13]

Unlike classical phase transition driven by thermal fluctuations, quantum phase transition of the many-body system is driven by pure quantum fluctuations. It is characterized by the abrupt changes in the properties of the ground state of the system, which results from the presence of the level crossing and avoid-crossing between the ground state and the excited state.[14] In the past few years, many methods were developed to study the QPT from different perspectives, such as quantum entanglement,[15] and quantum fidelity.[16] Since the features of energy-level crossings or avoided crossings correspond to the divergence or extremum property of the Berry curvature, the energy level structures can be captured by the geometric phase. This relationship has been observed experimentally in the two-spin XY model.[17] In this Letter, we report an observation of this phenomenon in a more complex many-body system, i.e., the three-spin XY model, and further study the relationship of the ground-state geometric phase and QPT. First, we analyze the ground-state geometric phases of the three-spin XY model. Then, we carry out the experiment with a four-spin NMR system and present the experimental results. Finally, a brief summary with a discussion is presented.

Consider the one-dimensional spin-1/2 XY model with three spins in a uniform external magnetic field,

$$H(\lambda,\gamma) = -\frac{\lambda}{2}\sum_{i=1}^{3}\sigma_z^i - \frac{1+\gamma}{2}\sum_{i=1}^{3}\sigma_x^i\sigma_x^{i+1} - \frac{1-\gamma}{2}\sum_{i=1}^{3}\sigma_y^i\sigma_y^{i+1}, \quad (1)$$

with periodic boundary condition, i.e., $\sigma_v^4 = \sigma_v^1$. Here $\sigma_{v(v=x,y,z)}^i$ denotes the Pauli operators of the

*Supported by the National Key Basic Research Program under Grant Nos 2013CB921800 and 2014CB848700, the National Science Fund for Distinguished Young Scholars under Grant No 11425523, the National Natural Science Foundation of China under Grant Nos 11375167, 11227901, 91021005 and 11575173, the Strategic Priority Research Program (B) of the Chinese Academy of Sciences under Grant No XDB01030400, the Research Fund for the Doctoral Program of Higher Education of China under Grant No 20113402110044, the China Postdoctoral Science Foundation, and the Fundamental Research Funds for the Central Universities.

**Corresponding author. Email: zkli@ustc.edu.cn; xhpeng@ustc.edu.cn

ith qubit, γ represents the anisotropy of the coupling strength, and λ denotes the external magnetic field in the z-direction. The lowest two energies of the system are $E_\pm = -1 \pm \frac{\lambda}{2} - \sqrt{(\lambda \pm 1)^2 + 3\gamma^2}$, with the corresponding orthonormalized eigenstates

$$|\psi\rangle_+ = \sin\left(\frac{\theta_+}{2}\right)|W\rangle_{001} + \cos\left(\frac{\theta_+}{2}\right)|111\rangle,$$
$$|\psi\rangle_- = \sin\left(\frac{\theta_-}{2}\right)|000\rangle + \cos\left(\frac{\theta_-}{2}\right)|W\rangle_{011}, \quad (2)$$

where $\tan(\theta_\pm/2) = [(\lambda\pm1)+\sqrt{(\lambda \pm 1)^2 + 3\gamma^2}]/(\sqrt{3}\gamma)$, $|W\rangle_{011} = \frac{1}{\sqrt{3}}(|011\rangle + |101\rangle + |110\rangle)$ and $|W\rangle_{001} = \frac{1}{\sqrt{3}}(|001\rangle + |010\rangle + |100\rangle)$.

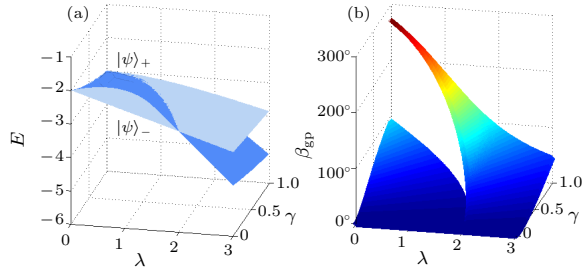

Fig. 1. Energy levels and geometric phases of the three-spin XY model. (a) The lowest two energies as functions of the isotropy parameter γ and magnetic field strength λ. The energy level crossing points between the ground state and the first excited state lie along the line $\gamma^2+(\lambda/2)^2 = 1$. (b) The geometric phase of the ground state $|\psi(0)\rangle_g$ in the plane of γ and λ. When $\gamma^2+(\lambda/2)^2 = 1$, the ground state is doubly degenerate and then the geometric phases associated change discontinuously.

To generate the geometric phases, we let the Hamiltonian adiabatically rotate around the z-axis with $U_z(\varphi) = \Pi_{k=1}^N e^{-i\frac{\varphi}{2}\sigma_z^k}$, the Hamiltonian can be written as $\tilde{H}(\lambda,\gamma,\varphi) = U_z^\dagger(\varphi)H(\lambda,\gamma)U_z(\varphi)$, which has the same spectrum as Eq. (1). The quantum adiabatic theorem predicts that a system initially in one of its eigenstates $|\psi(0)\rangle_g$ will remain in its instantaneous eigenstate $|\psi(\varphi)\rangle_g$ of the Hamiltonian $\tilde{H}(\lambda,\gamma,\varphi)$ in this progress. As a result, the cyclic adiabatic evolution from 0 to π along the closed path C_1 lets the Hamiltonian and quantum state return to their original forms in the parameter space. The ground state of the studied system is

$$|\psi(\varphi)\rangle_g = \begin{cases} \sin\left(\frac{\theta_+}{2}\right)|W\rangle_{001} \\ +e^{-i2\varphi}\cos\left(\frac{\theta_+}{2}\right)|111\rangle, \ \xi \le 1, \\ \sin\left(\frac{\theta_-}{2}\right)|000\rangle \\ +e^{-i2\varphi}\cos\left(\frac{\theta_-}{2}\right)|W\rangle_{011}, \ \xi > 1 \end{cases}, \quad (3)$$

where $\xi \equiv \gamma^2 + (\lambda/2)^2$. According to the standard Berry's formula $\beta_{gp} = i\oint_{\phi:0\to\pi}\langle\psi|\partial_\phi|\psi\rangle$, the adiabatic path C_1 will generate the geometric phase

$$\beta_{gp} = \begin{cases} \pi(1+\cos(\theta_+)), & \xi \le 1 \\ \pi(1+\cos(\theta_-)), & \xi > 1 \end{cases}. \quad (4)$$

For $0 < \gamma < 1$, the geometric phases have an abrupt change along the energy cross line $\gamma^2 + (\lambda/2)^2 = 1$. A special case is the XX spin model (i.e., $\gamma = 0$). Since the operation $U_z(\varphi)$ does not change the Hamiltonian of the system, the geometric phases vanish as shown in Fig. 1(b).

Apart from the geometric phase, the dynamic phase will also be generated relative to the instantaneous energy of the system $\beta_{dp} = i\oint E(t)dt$. To eliminate the dynamical phase in experiment, we construct another evolution path C_2 $\tilde{H}'(\lambda,\gamma,\varphi) = -\tilde{H}(\lambda,\gamma,\varphi)$, which will generate the same geometric phase and the opposite dynamical phase as path C_1.[3] Then the contribution of the dynamical phase is eliminated and only the geometric phase will be acquired. Here we introduce an ancilla qubit coupled to the system. The auxiliary qubit is initialized into a superposition state $\frac{1}{\sqrt{2}}(|0\rangle + |1\rangle)$, and the controlled operation $V_k = |0\rangle\langle 0|_a \otimes I_8 + |1\rangle\langle 1|_a \otimes U_k$ is implemented, where I_8 represents an 8×8 unit operator and the unitary operator U_k is the cyclic adiabatic evolution along the chosen path of the system. When U_k creates a nonzero phase, it will effectively introduce a relative phase shift between $|0\rangle$ and $|1\rangle$, which can be detected in experiment. The quantum circuit is presented in Fig. 2.

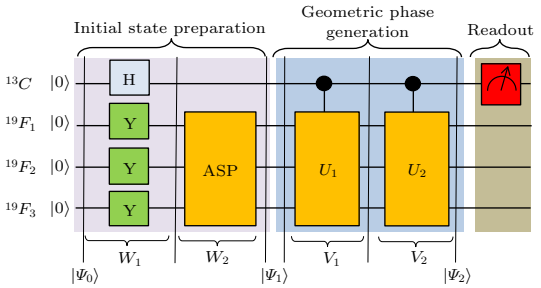

Fig. 2. Quantum circuit of the experimental progress. Here Y and H represent the operation $e^{i\frac{\pi}{4}\sigma_y}$ and Hadamard gate, respectively, and ASP denotes adiabatic preparation of the ground state $|\psi(0)\rangle_g$. Notice that $|\psi(0)\rangle_g = |\psi(\pi)\rangle_g$, U_1 and U_2 are two adiabatic evolutions, $|\Psi_{i(i=0,1,2)}\rangle$ represents the expected instantaneous state of the whole system, where $|\Psi_0\rangle = |0000\rangle$, $|\Psi_1\rangle = \frac{1}{\sqrt{2}}(|0\rangle + |1\rangle)\otimes|\psi(0)\rangle_g$, and $|\Psi_2\rangle = \frac{1}{\sqrt{2}}(|0\rangle + e^{i2\beta_{gp}}|1\rangle)\otimes|\psi(\pi)\rangle_g$.

The experiment was carried out on a Bruker AV-400 MHz spectrometer (9.4 T) at room temperature. We chose iodotrifluoroethylene dissolved in d-chloroform as a four-qubit quantum system, where a ^{13}C nucleus is labeled as the ancilla qubit and three ^{19}F nuclei are used to simulate the XY model. The natural abundance of the sample with a single ^{13}C is about 1%. To distinguish those molecules against the large background, we read out all three ^{19}F qubits via the ^{13}C channel. The natural Hamiltonian of the system in the double rotating frame is

$$H_{nmr} = \sum_{i=1}^{4}\frac{\omega_i}{2}\sigma_z^i + \sum_{i<j,=1}^{4}\frac{\pi J_{ij}}{2}\sigma_z^i\sigma_z^j, \quad (5)$$

where ω_i is the chemical shift of spin i, and J_{ij} is the scalar coupling constant between spins i and j. Figure 3 shows the measured properties of this four-qubit quantum system. As summarized, this experiment includes three steps: (i) initial state preparation: prepare the ground state of the XY spin model of $H(\lambda,\gamma)$; (ii) geometric phase generation: drive the system evolving along the engineered paths; and (iii) readout: measure the geometric phases.

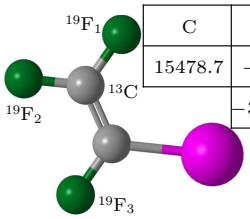

	C	F_1	F_2	F_3		T_2 (s)
	15478.7	−297.6	−257.6	39.1	C	7.9
		−33114.5	64.6	51.4	F_1	4.4
			−42674.9	−129.1	F_2	6.8
				−56450.7	F_3	6.8

Unit: (Hz)

Fig. 3. Molecular structure and relevant parameters of iodotrifluoroethylene at 303 K. The chemical shifts and J-coupling constants are on and above the diagonal in the table, respectively. The spin-lattice relaxation times T_1 are 21 s for ^{13}C and 12.5 s for ^{19}F. The chemical shifts are given with respect to reference frequencies of 376.47 MHz (fluorines) and 100.64 MHz (carbon). The transmitter offsets of carbon channel and fluorine channel are set at 15478.7 Hz and −44701.0 Hz, respectively.

(i) Initial state preparation, starting from the equilibrium state, we first initialized the system into the pseudopure state with the line-selective-transition method[17]

$$\rho_{\rm pps} = \frac{1-\varepsilon}{16} I_{16} + \varepsilon |0000\rangle\langle 0000|, \tag{6}$$

where I_{16} represents the 16×16 unity operator and $\grave{o} \approx 10^{-5}$ is the polarization. The NMR spectrum and experimentally measured density matrix of the pseudopure state are shown in Fig. 4. To create the ground state of the Hamiltonian $H(\lambda,\gamma)$, we designed an adiabatic path starting with an initial Hamiltonian $H_0 = \sum_{i=2}^{i=4} \sigma_x^i$, whose ground state is known as $|\phi\rangle = \frac{1}{2}(|0\rangle - |1\rangle)^{\otimes 3}$. In the experiment, $|\phi\rangle$ can be easily prepared by the operation

$$W_1 = \frac{1}{\sqrt{2}} \begin{pmatrix} 1 & 1 \\ 1 & -1 \end{pmatrix} \otimes e^{\frac{i\pi}{4}\sum_{i=2}^{4}\sigma_y^i}. \tag{7}$$

Notice that the ancilla qubit was prepared into the superposition state $\frac{1}{\sqrt{2}}(|0\rangle + |1\rangle)$ by a Hadamard gate at the same time.

Next we use the adiabatic evolution to drive the system into the ground state of the Hamiltonian. A time-dependent Hamiltonian $H_{\rm ad}(t)$ smoothly interpolates between H_0 and $H(\lambda,\gamma)$: $H_s(t) = [1 - s(t)]H_0 + s(t)H(\lambda,\gamma)$, where the function $s(t)$ varies from 0 to 1 to parameterize the interpolation. If the quantum system starts initially in its ground state of $H(0)$ and the variation of $H_s(t)$ is adiabatic, the final state will be close to the ground state of $H(\lambda,\gamma)$. To ensure that the system is prepared in the ground state of $H(g,\gamma)$, the sufficiently slow variation of $H_{\rm ad}(t)$ means that the traditional adiabatic condition $|\frac{\langle\psi_{\rm g}(t)|\dot{\psi}_{\rm 1e}(t)\rangle}{\varepsilon_{\rm 1e}(t)-\varepsilon_{\rm g}(t)}| \ll 1$ is fulfilled, where $\psi_{\rm g}(t)$ and $\psi_{\rm 1e}(t)$ refer to the instantaneous ground state and the first excited state, respectively, and $\varepsilon_{\rm g}(t)$, $\varepsilon_{\rm 1e}(t)$ are the corresponding energies. An optimal function of $s(t)$ determines the efficiency of initial state preparation. To find the optimal interpolation function $s(t)$ for the adiabatical evolution process, we rewrite the adiabatic condition as

$$\left|\frac{ds(t)}{dt}\right| \ll \frac{|\varepsilon_{\rm 1e}(t) - \varepsilon_{\rm g}(t)|^2}{\left|\langle\psi_{\rm g}(t)|\frac{\partial H_{\rm ad}(s)}{\partial s}\right||\psi_{\rm 1e}(t)\rangle} = \chi, \tag{8}$$

which defines the optimal sweep of the control parameter $s(t)$ with the scan speed $\frac{ds(t)}{dt}$. The required time dependence of $s(t)$ was numerically optimized for constant adiabaticity parameter $\kappa = \frac{ds}{dt}/\chi$. The time dependence of $s(t)$ was chosen such that the adiabaticity parameter $\kappa < 0.25$ at all times.

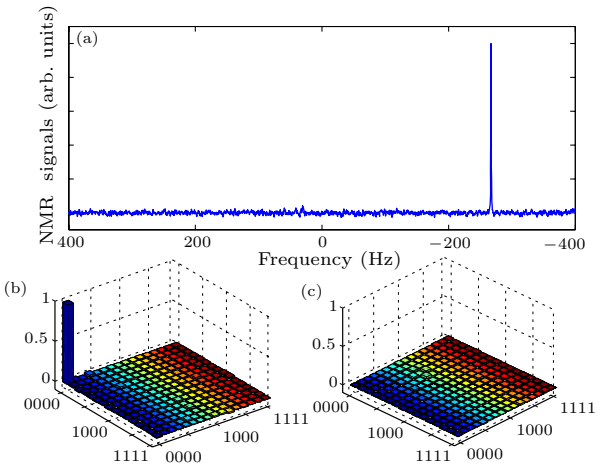

Fig. 4. Experimental spectrum and density matrix of the pseudopure state. (a) The ^{13}C spectra after a $e^{-i\frac{\pi}{4}\sigma_y}$ readout pulse applied to the initial pseudopure state. (b), (c) The real and imaginary parts of experimental density matrix of the pseudopure state. The rows and columns represent the standard computational basis in binary order from $|0000\rangle$ to $|1111\rangle$. The fidelity is about 0.99.

In the experiment, we need to discretize $H_s(t)$ into L-segment interpolated between H_0 and $H(\lambda,\gamma)$: $H_s[l] = [1 - s(l)]H_0 + s(l)H(\lambda,\gamma)$, where the function $s(l)$ varies from 0 to 1. The evolution operator for the lth step is given by $e^{-i\tau H_s[l]}$, where $\tau = T_0/L$ and T_0 is the total evolved time. The system will evolve according to the unitary operator

$$W_2 = \prod_{l=1}^{L} e^{-i\tau H_s[l]}. \tag{9}$$

We use a numerical procedure for optimizing the parameter $s(l)$ to make the operation W_2 have the theoretical efficiency above 0.995. In experiment, the unitary operators $W_{1,2}$ were realized by shaped quantum

control pulses found by the gradient ascent pulse engineering (GRAPE) technique,[19] with the length of each pulse being 25 ms and the number of segments being 2500. All the pulses have theoretical fidelities over 0.99 and are designed to be robust against the inhomogeneity of radio-frequency pulses.

(ii) Geometric phase generation, to perform the adiabatic rotation of the Hamiltonian around the z-axis, we discretize the continuous adiabatic passage into M segments with the instantaneous Hamiltonian $\tilde{H}[m] = (e^{-\frac{im\pi}{M}\sum_{i=2}^{4}\frac{1}{2}\sigma_z^i})^\dagger H(g,\gamma)(e^{-\frac{im\pi}{M}\sum_{i=2}^{4}\frac{1}{2}\sigma_z^i})$. The system will evolve according to the unitary operator $U_1 = \prod_{m=1}^{M} e^{-it\tilde{H}[m]}$, where $t = T/M$ and T represents the total evolution time. To ensure the success of the adiabatic evolution in experiment, we use numerical simulation to optimize M and T, thus the efficiency keeps above 0.995. For instance, at the point $(\lambda,\gamma) = (1.55, 0.6)$ the parameters are optimized as $M = 30$ and $T = 9.14$.

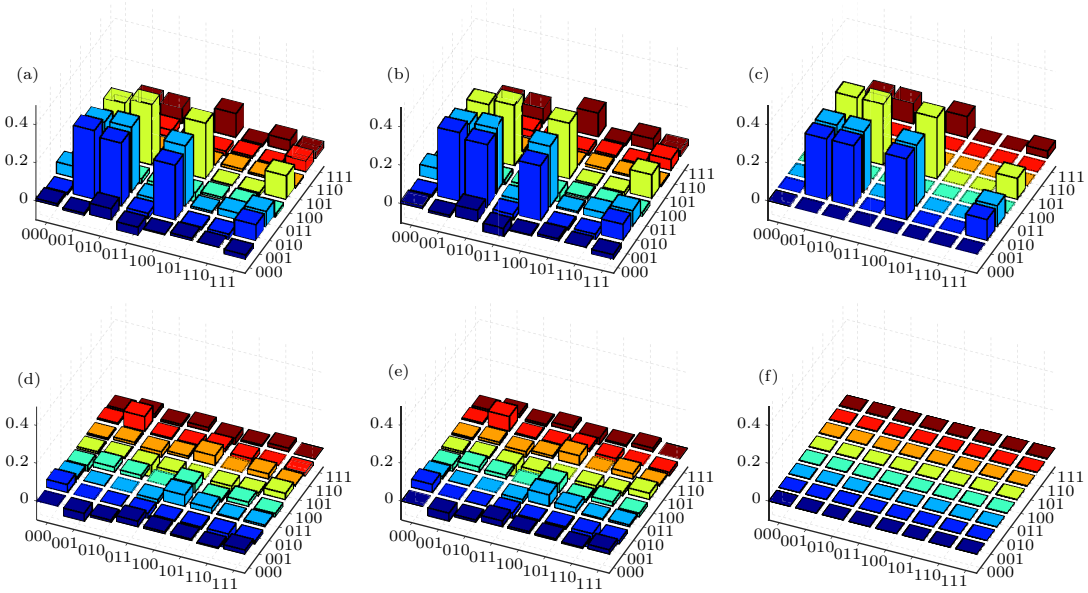

Fig. 5. (a), (d), (b), (e) Experimental density matrix before and after the adiabatic evolutions at the point $(\lambda,\gamma) = (1.55, 0.6)$. (c), (f) Theoretical density matrix. The top and bottom denote the real and imaginary components, respectively. Notice that the ancilla qubit is traced over.

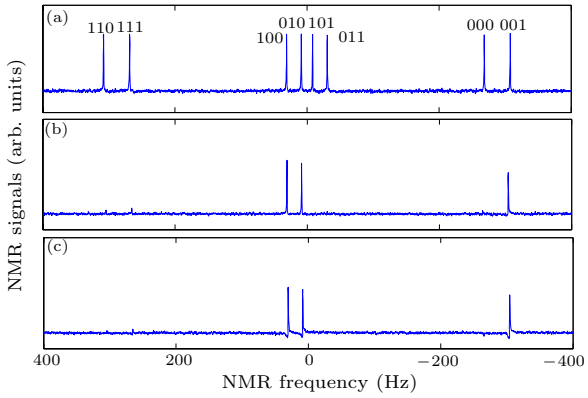

Fig. 6. (a) The experimental ^{13}C spectra of the thermal equilibrium state. The eight resonance lines are labeled by the corresponding states of the other three qubits. (b), (c) The experimental ^{13}C spectra of the state before and after the adiabatic evolutions at the point $(\lambda,\gamma) = (1.55, 0.6)$.

The second adiabatic passage C_2 can be implemented with the same method, and the corresponding propagator is written as $U_2 = \prod_{m=1}^{M} e^{-it\tilde{H}'[m]}$. Taking consideration of the ancilla qubit, the control operations can be written as

$$V_{k(k=1,2)} = |0\rangle\langle 0| \otimes I_8 + |1\rangle\langle 1| \otimes U_k, \qquad (10)$$

which can be achieved by using standard pulsed NMR techniques in theory. However, in experiment direct implementation of the gate operation $V_{1,2}$ will need a large number of single-qubit operations and free evolutions, which will accumulate systematic errors and significant decoherence effect. To overcome these problems and to reach a high-fidelity quantum coherent control, V_1 and V_2 are realized by two GRAPE pulses individually in experiment, with theoretical fidelities over 0.99 and pulse length being 25 ms. To examine if the final state is still in the ground state, the quantum state tomography technique could be used at the beginning and end of the adiabatic evolutions. For example, at the point $(\lambda,\gamma) = (1.55, 0.6)$ the experimental fidelities before and after the two adiabatic evolutions are about 0.96 and 0.93. The fidelity is defined by $F = \frac{\mathrm{Tr}(\rho_{\mathrm{exp}}\rho_{\mathrm{th}})}{\sqrt{\mathrm{Tr}(\rho_{\mathrm{exp}}^2)\mathrm{Tr}(\rho_{\mathrm{th}}^2)}}$, where ρ_{exp} and ρ_{th} represent the experimentally measured density matrix and the ideal expectation, respectively. Figure 5 gives the corresponding tomography results of the reduced

density matrices by partially tracing over the ancilla qubit.[20]

(iii) Readout, the final state $|\Psi_2\rangle = \frac{1}{\sqrt{2}}(|0\rangle + e^{i2\beta_{\rm gp}}|1\rangle) \otimes |\psi(\pi)\rangle_{\rm g}$ will lead to a relative phase shift between $|0\rangle$ and $|1\rangle$ of the auxiliary qubit. Taking the input state $|\Psi_1\rangle = \frac{1}{\sqrt{2}}(|0\rangle + |1\rangle) \otimes |\psi(0)\rangle_{\rm g}$ as the reference spectrum, we measure the relative phase information by the phase of the Fourier-transformed spectra.[21] Figure 6 shows an example of the phase measurement at the point $(\lambda, \gamma) = (1.55, 0.6)$, in which Figs. 6(b) and 6(c) correspond to the spectra of the state before and after the two adiabatic evolutions. In the situation $\gamma^2 + (\lambda/2)^2 < 1$, the ground state of the system is $|\psi(0)\rangle_{\rm g} = \sin(\frac{\theta_+}{2})|W\rangle_{001} + \cos(\frac{\theta_+}{2})|111\rangle$. Four resonance lines corresponding to this state are visible in the NMR spectrum as shown in Fig. 6. In the initial state the four lines appear in absorption, corresponding to the reference phase (equal to zero). During the adiabatic evolution, the system will acquire a phase $2\beta_{\rm gp}$. By numerical analysis of the spectra, we find $\beta_{\rm gp} \approx 10.8°$, which is close to the theoretically expected value of 13.3°.

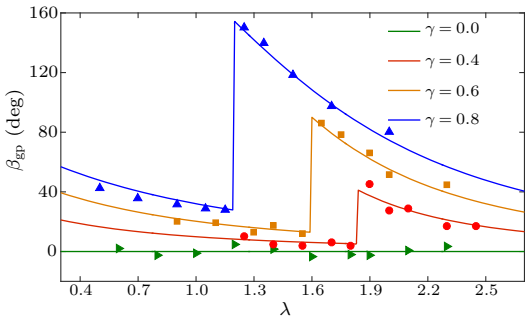

Fig. 7. Experimentally measured geometric phases (symbols) for different anisotropy parameters γ and external fields λ, along with the theoretical expectations (solid lines).

The experimentally measured geometric phases as a function of λ are presented in Fig. 7. The symbols show the experimental data points and the solid lines represent the theoretically expected geometric phases for different γ. We find that the observed geometric phases present an abrupt change near the energy-level crossing point $g = 2\sqrt{1-\gamma^2}$, which agrees with the theoretical expectation. As for the XX spin model (i.e., $\gamma = 0$), the results of the experiment are close to the theoretically expected value of zero.

In experiment, the average error is about 4°, which mainly comes from the imperfection of the pseudopure state and the GRAPE pulses. Using the experimentally reconstructed density matrix, we find that the imperfection of pseudopure state contributes about 1° to the errors. Moreover, numerical simulations reveal that the imperfection of the four GRAPE pulses implemented on the ideal pseudopure state will produce about 1° error in total. The duration of each experiment is about 100 ms, which is short compared with the relaxation time $T_2^* \approx 1.2$ s. Therefore, the effect of decoherence should be relatively small. The remaining errors may result from the inhomogeneities of radio-frequency fields, static magnetic fields and the variations of the chemical shifts.

In summary, using the NMR quantum simulator we have observed the ground-state geometric phase of the three-spin XY model. The experimental results imply that the geometric phase can be used to characterize the quantum phase transition of many-body systems with no need to undergo it. This work will contribute to an improved understanding of the ground-state properties and QPT for many-body quantum systems. In future, this method could be extended to larger and more general spin systems for studying different types of phase transition.

References

[1] Berry M V 1984 *Proc. R. Soc.* A **329** 45
[2] Samuel J and Bhandari R 1988 *Phys. Rev. Lett.* **60** 2339
[3] Aharonov Y and Anandan J 1987 *Phys. Rev. Lett.* **58** 1593
[4] Sjöqvist E, Pati A K, Ekert A, Anandan J S, Ericsson M, Oi D K L and Vedral V 2000 *Phys. Rev. Lett.* **85** 2845
[5] Tong D M, Sjöqvist E, Kwek L C and Oh C H 2004 *Phys. Rev. Lett.* **93** 080405
[6] Tomita A and Chiao R Y 1986 *Phys. Rev. Lett.* **57** 937
[7] Bitter T and Dubbers D 1987 *Phys. Rev. Lett.* **59** 251
[8] Suter D, Mueller K T and Pines A 1988 *Phys. Rev. Lett.* **60** 1218
[9] Leek P J, Fink J M, Blais A, Bianchetti R, Göppl M, Gambetta J M, Schuster D I, Frunzio L, Schoelkopf R J and Wallraff A 2007 *Science* **318** 1889
[10] Morpurgo A F, Heida J P, Klapwijk T M, van Wees B J and Borghs G 1998 *Phys. Rev. Lett.* **80** 1050
[11] Niu Q, Wang X, Kleinman L, Liu W M, Nicholson D M C and Stocks G M 1999 *Phys. Rev. Lett.* **83** 207
[12] Jones J A, Vedral V, Ekert A and Castagnoli G 2000 *Nature* **403** 869
[13] Zhu S L 2006 *Phys. Rev. Lett.* **96** 077206
[14] Sachdev S 1999 *Quantum Phase Transitions* (Cambridge: Cambridge University Press)
[15] Osterloh A, Amico L, Falci G and Fazio R 2002 *Nature* **416** 608
[16] Zhang J, Peng X, Rajendran N and Suter D 2008 *Phys. Rev. Lett.* **100** 100501
[17] Peng X, Wu S, Li J, Suter D and Du J 2010 *Phys. Rev. Lett.* **105** 240405
[18] Peng X, Zhu X, Fang X, Feng M, Gao K, Yang X and Liu M 2001 *Chem. Phys. Lett.* **340** 509
[19] Khaneja N, Reiss T, Kehlet C, Schulte-Herbruggen T and Glaser S J 2005 *J. Magn. Reson.* **172** 296
[20] Lee S J 2002 *Phys. Lett.* A **305** 349
[21] Ernst R R, Bodenhausen G and Wokaun A 1987 *Principles of Nuclear Magnetic Resonance in One and Two Dimensions* (Oxford: Oxford University Press)